EUROPEAN ORGANIZATION FOR NUCLEAR RESEARCH

CERN-PPE/96-95
July 8, 1996

Search for neutral Higgs boson production through the process $e^+e^- \to Z^* H^0$

The L3 Collaboration

Abstract

The results of the searches for neutral Higgs boson production in the process $e^+e^- \to Z^* H^0$ are reported, focusing on Higgs boson masses below 70 GeV. The data sample consists of three million hadronic Z decays collected by the L3 experiment at LEP from 1991 through 1994. No signal is found leading to a lower limit on the mass of the Standard Model Higgs boson of 60.2 GeV at 95% C.L.

These results are also interpreted in the framework of the General Two Doublet Model and limits on the non standard Higgs boson production through the process $e^+e^- \to Z^*h^0$ are set. A lower limit of 66.7 GeV at 95% C.L. is obtained for the case where the Higgs decays into an invisible final state.

Submitted to *Phys. Lett. B*

Introduction

The Standard Model [1] predicts the spontaneous breaking of $SU(2)_L \otimes U(1)_Y$ by means of a doublet of complex scalar fields ϕ. Due to the ϕ vacuum expectation value (v.e.v.) the W and Z bosons acquire their masses at the expense of three degrees of freedom of the field ϕ. The last degree of freedom is taken by a neutral scalar particle: the Higgs boson [2]. In the framework of this model the couplings of the H^0 boson to the fermions and to the gauge vector bosons are known but its mass is not predicted. The main production mechanism of the Higgs boson at LEP is predicted to be through the decay of the Z boson into an H^0 and a virtual Z^* [3], $\mathrm{e}^+\mathrm{e}^- \rightarrow \mathrm{Z} \rightarrow \mathrm{H}^0 + \mathrm{Z}^* \rightarrow \mathrm{H}^0 + \mathrm{f}\bar{\mathrm{f}}$.

A heavy Higgs boson, with a mass between 10 and 100 GeV, decays predominantly into a $\mathrm{b}\bar{\mathrm{b}}$ pair, although the branching ratios into $\mathrm{c}\bar{\mathrm{c}}$ and $\tau^+\tau^-$ are not negligible. In this paper we use the latest theoretical calculations [4, 5] of full one loop radiative corrections for the Standard Model Higgs production and decay.

In two doublet models, where five scalar physical Higgs bosons are predicted (two charged $\mathrm{H}^+\mathrm{H}^-$, two neutral CP even, H^0 and h^0, where the latter is the lightest among the two, and one neutral CP odd A^0), the bremsstrahlung process $\mathrm{e}^+\mathrm{e}^- \rightarrow \mathrm{Z}^*\mathrm{h}^0$ is still possible, but one has to take into account a model dependent factor which reduces the production rate. In the Minimal Supersymmetric Standard Model (MSSM [6]) this factor is equal to $\sin^2(\beta - \alpha)$ where α is the mixing parameter in the CP even Higgs sector while $\tan\beta$ is the ratio between the v.e.v. of the two Higgs doublets.

In two doublet models the decays of the h^0 depend on many parameters. The branching ratios for the decay into different fermions depend on $\tan\beta$ and α. If kinematically allowed the decay into a pair of A^0 may be dominant, thus leading, especially for A^0 masses close to half h^0 mass, to a different signature with respect to the standard bremsstrahlung process. In addition, the h^0 may decay into invisible final states [7], for instance into a pair of χ_1^0, where χ_1^0 is the lightest neutralino, supposed to be the lightest supersymmetric particle and to be stable in R parity conserving supersymmetric models.

The results of earlier searches for a Higgs boson have been published by all the LEP experiments [8–11]. We present here the updated results, obtained with all the statistics collected through 1994 around the Z peak, on the search for bremsstrahlung production of the Higgs boson in the $\mathrm{H}^0\nu\bar{\nu}$, $\mathrm{H}^0\mathrm{e}^+\mathrm{e}^-$ and $\mathrm{H}^0\mu^+\mu^-$ channels in the framework of the Standard Model and in the General Two Doublet Model, for Higgs masses smaller than 70 GeV. We also report on the search for invisible Higgs decays never performed before by L3.

1 The L3 Detector

The L3 detector [12] consists of a silicon microstrip detector [13], a central tracking chamber (TEC), a high resolution electromagnetic calorimeter composed of BGO crystals, a lead–scintillator ring calorimeter at low polar angles [14] (ALR), a scintillation counter system, a uranium hadron calorimeter with proportional wire chamber readout, and an accurate muon chamber system. These detectors are installed in a 12 m diameter magnet which provides a solenoidal field of 0.5 T and an additional toroidal field of 1.2 T in the forward backward region. The luminosity is measured using BGO calorimeters preceded by silicon trackers [15] situated on each side of the detector.

2 Data Sample and Simulation

In these analyses we use 3.05 million hadronic Z decays, corresponding to approximately 114 pb^{-1} of integrated luminosity collected by the L3 experiment in the period from 1991 through 1994.

An extensive study of the main background sources is performed using Monte Carlo generated events: we simulate hadronic Z decays with `JETSET` [16] and `HERWIG` [17], hadronic events with semileptonic decays of the b quark with `JETSET`, two photon interactions with `DIAG36` [18] and `LEP4F` [19], $\tau^+\tau^-$events with `KORALZ` [20], Bhabha events with `BHAGENE3` [21] and all possible final states for the four fermion processes with `FERMISV` [22] .

The Monte Carlo statistics for hadronic Z decays and two photon interactions is about twice the statistics of the whole data sample, while for the other processes it is many times the statistics of the data. The detector response is fully simulated and additional time dependent detector inefficiencies are taken into account.

3 $\mathrm{H}^0\nu\bar{\nu}$ Channel

3.1 Event Reconstruction

Hadronic events are reconstructed using the information coming from all the subdetectors. The energy of the event is obtained taking into account the energy deposition in the calorimeters and the momentum measured by TEC and the muon chambers. The algorithm [23] takes into account the difference between neutral and charged clusters by different calibration constants.

The distinctive signature of the $\mathrm{H}^0\nu\bar{\nu}$ channel is the missing energy and two acollinear jets, or three jets not lying in the same plane, with no hadronic activity recoiling against the Higgs decay products. With increasing Higgs mass these characteristics become less evident and events become very similar to $\mathrm{b}\bar{\mathrm{b}}$ events and to $\mathrm{q}\bar{\mathrm{q}}\gamma$ events with the photon escaping detection.

Events are reconstructed by dividing the space into two hemispheres separated by a plane perpendicular to the thrust axis and forming a jet in each hemisphere. We define the acollinearity as the angle in space between the two jets and the acoplanarity as the angle between the two jets projected onto the $R-\phi$ plane. In order to discriminate between the signal and the background the following variables are used in the selection procedure:

- the visible energy (E_{vis}),
- the total transverse momentum of the event ($P_{\perp}$),
- the total parallel momentum of the event ($P_{||}$),
- the polar angle of the missing momentum of the event (θ_{miss}),
- the jet energies (E_{jet1} and E_{jet2}),
- the jet polar angles (θ_{jet1} and θ_{jet2}),
- the energy deposition in a cone of 60° half opening angle around the vector opposite to the sum of the two jet directions in space (E^{b}_{60}),
- the energy deposition ($\not{E}^{\perp}_{25}$) and the number of tracks (N^{tk}_{25}) within $\pm 25°$ of the missing momentum direction in the $R-\phi$ plane,

- the ratio between the scalar sum of the particle momenta transverse to the jet direction and the jet energy ($y^{\perp} = \sum p_{\perp}/E_{jet}$), for the narrow jet ($y^{\perp}_{N}$) and the broad jet ($y^{\perp}_{B}$), where the broad jet is by definition the one with the largest ratio $y^{\perp}$,

- the sum of the angles between the jets (θ_{123}) when the event is forced into three jets using the `LUCLUS` [16] algorithm,

- the energy deposition in a cone of 25° half opening angle around the missing momentum direction ($\not{E}_{25}$),

- the generalized acoplanarity α^G, defined as: $\pi - [\sin(\min(\theta_{jet_1}, \theta_{jet_2})) \times (\pi - \text{acoplanarity})]$.

3.2 Study of Physics and Instrumental Backgrounds

In order to identify the main sources of physics background and to optimize the choice of the variables to be used, a Monte Carlo study at the generator level is done. Using a selection similar to the final one but with looser cuts we reduce the $\mathrm{q\bar{q}}$ background by a factor $2 \cdot 10^5$. Half of the events passing this preselection consist of Z decays into $\mathrm{b\bar{b}}$ with the following features: energetic neutrinos from semileptonic decays with a transverse momentum with respect to the b quark of more than 1 GeV and often accompanied by a hard initial state photon lost in the beam pipe. Other hadronic Z decays pass this selection mainly when they are badly measured due to the presence of very energetic (more than 10 GeV) neutral long lived hadrons.

Besides the physics background, detector inefficiencies can also lead to a missing energy signature thus faking signal events. The $\mathrm{q\bar{q}}\gamma$ events with the photon hitting an inefficient region in the electromagnetic calorimeter constitute the most severe source of instrumental background. To study its influence a special reconstruction is applied to $\mathrm{q\bar{q}}\gamma$ events. An electromagnetic cluster, identified as a photon, is removed from the reconstruction and the event is then subjected to $\mathrm{H}^0\nu\bar{\nu}$ selection. Figure 1 shows the comparison of the data with the Monte Carlo expectations for resolution on the missing momentum direction and on the hadronic mass, as well as the energy and the angular distributions of the radiated photon for the selected events. In all these distributions we observe a good agreement between the data and the simulated events.

The $\mathrm{q\bar{q}}\gamma$ background requires a specific rejection. Namely the missing momentum must not point to a dead BGO region within 20° from its edge (to allow for angular resolution of missing momentum) and E^b_{60} must be less than 2 GeV. The cut on the missing momentum direction suppresses the $\mathrm{q\bar{q}}\gamma$ background due to dead BGO regions by a factor 10 with an average loss of Higgs detection efficiency of 7.8%. The second cut rejects 60% of the remaining background and introduces an extra 2.4% inefficiency to the signal. At this stage the expected $\mathrm{q\bar{q}}\gamma$ background is reduced to approximately 0.35 events.

3.3 Final Selection Procedure

Two important issues for the Higgs searches are the *a priori* choice of the selection criteria and the correct estimate of the expected background after the selection is applied. The method [23] used in the present analysis addresses both these issues.

First, the search sensitivity is defined as the ratio of the signal efficiency and the average Poisson upper limit on the signal,

$$\varepsilon / \sum_{n=0}^{\infty} k_n P_b(n)$$

where k_n is the 95% C.L. Poisson upper limit for n observed events, $P_b(n)$ is the Poisson distribution for observing n events with a background of b events and ε is the signal efficiency. The parameters b and ε are functions of the cut values. Parameter b in addition depends on the data statistics. In order to obtain the analytical parametrization of these functions using limited Monte Carlo statistics the number of variables is reduced to one in the following manner: for a given set of ranges of cuts X^i_{loose} and X^i_{tight} (where $i = Cut_1, ..., Cut_N$) we define a variable ξ which runs from 0 to 1, and is linearly related to all the cut values such that when ξ is 0 all the cuts are on the loose edge (many background events satisfy the selection) and when it is 1 all the cuts are on the tight edge (no or few background events pass the selection):

$$X^i_{cut} = X^i_{loose} + (X^i_{tight} - X^i_{loose}) \times \xi.$$

Then, we parametrize $b(\xi)$ with a steeply falling analytical function and find that both exponential and Gaussian functions provide a satisfactory description. The validity of the parametrization is verified using a statistically independent Monte Carlo sample. In practice the loose-edge values for all cuts are fixed by the preselection and the parametrization is done for various tight-edge values used in the next step.

The search sensitivity is maximized by varying the tight-edge values for all the cuts using the MC expectations for the signal and the background as an input to the minimization program `MINUIT` [24]. In this way the correlations between the variables are taken into account thus exploiting the full discriminating power of a set of variables. As a result of this procedure the optimal cut values are defined without using data at all.

3.4 Mass Range 50 GeV $< M_H <$ 70 GeV

A preselection of data [23] is performed in order to reject badly reconstructed events and beam gas interactions as well as Z decays with little missing energy. This has a very small effect on the Higgs signal and is based upon minimal requirements on the energy released in the calorimeters and on the quality of the charged tracks. Next, $\tau^+\tau^-$ events are rejected by requiring at least 6 charged tracks and 15 calorimetric clusters. The following cuts are then applied in order to reject $e^+e^-q\bar{q}$ events produced in two photon interactions. We require less than 15 GeV in the luminosity monitor, the transverse momentum ($P_\perp$) greater than 7 GeV, $P_\perp/E_{\mathrm{vis}}$ greater than 0.13, $P_{||}/E_{\mathrm{vis}}$ less than 0.4, $E_{\mathrm{vis}}/\sqrt{s}$ greater than 0.45, $\sin(\theta_{miss})$ greater than 0.4 and $\min(E_{jet1}, E_{jet2})/E_{\mathrm{vis}}$ greater than 0.25. After this preselection the remaining background is composed of hadronic Z decays (98%) and of $e^+e^-q\bar{q}$ events (2%) with a negligible contribution of $\tau^+\tau^-$ events.

Finally from the procedure explained in the previous section, using a 60 GeV Higgs for optimization, we obtain the cut values given in Table 1. No events satisfy the final selection. The background from $\tau^+\tau^-b\bar{b}$ is estimated to be 0.02 events and that from $\nu\bar{\nu}q\bar{q}$ to be 0.01 events. These two processes constitute a small irreducible background and are not used in the optimization procedure described in the previous section. The number of expected $q\bar{q}$ background events is estimated to be 0.25 using the analytical approximation.

Figure 2-a shows the distribution of the number of events as a function of the variable ξ for the final choice of the cut ranges. The arrow shows the position of the ξ value determined by the optimization procedure which maximizes the search sensitivity.

The signal efficiencies for a Higgs mass ranging from 50 GeV to 70 GeV are shown in Table 2 together with the efficiencies in the other channels and the other mass ranges analysed. The

High mass $H^0\nu\bar{\nu}$ selection			
acollinearity	$<$	2.77	rad
acoplanarity	$<$	2.97	rad
θ_{123}	$<$	5.86	rad
$y_N^{\perp}$	$<$	0.494	
$y_B^{\perp}$	$<$	0.621	
$\not{E}_{25}$	$<$	0.74	GeV
$\not{E}_{25}^{\perp}$	$<$	7.83	GeV
$\min(\sin(\theta_{\mathrm{jet1}}), \sin(\theta_{\mathrm{jet2}}))$	$>$	0.4	

Table 1: Values of the cuts for the $50 \div 70$ GeV $H^0\nu\bar{\nu}$ selection determined with the optimization procedure described in the text.

Higgs mass (GeV)	2	5	9	15	20	30	40	50	60	65	70
$H^0\nu\bar{\nu}$ ε (%)	20.1	26.3	28.6	29.6	33.0	42.3	42.0	34.8	26.6	16.0	9.2
$H^0e^+e^-$ ε (%)	16.0	39.4	46.4	50.8	51.6	44.7	48.7	46.6	42.2	39.9	35.8
$H^0\mu^+\mu^-$ ε (%)	8.5	21.7	27.6	25.7	29.5	37.0	37.1	36.1	32.3	26.2	3.3

Table 2: Selection efficiencies for Higgs events in $H^0\nu\bar{\nu}$, $H^0e^+e^-$and $H^0\mu^+\mu^-$channels, as a function of the Higgs mass.

signal efficiency for $M_H = 60$ GeV is shown in Figure 2-b as a function of the number of expected events from the background.

The systematic uncertainty on the number of expected Higgs events arises from the uncertainty on the signal efficiency calculation, the theoretical calculation of the Higgs boson production cross section and branching fractions and the number of hadronic Z decays used for the normalization.

The systematic uncertainty on the signal efficiency calculation arises from the calibration procedure. The effect of the energy calibration is estimated by Gaussian smearing of the global energy scale by 3% and the energy scales of the individual subdetectors by 5%. These numbers are derived from a comparison between the calibration constants obtained using **JETSET** and **HERWIG**. The effect of the uncertainty in the angular resolution is evaluated by smearing the jet directions by 0.7° for θ and 1.7° for ϕ. This is derived from the comparison of data and Monte Carlo $q\bar{q}$ events. The overall effect on the efficiency for a 60 GeV Higgs signal is estimated to be 0.35%.

Other systematic errors on the number of expected Higgs events are estimated to be the following: less than 1% due to the theoretical uncertainty on the Higgs boson production cross section; less than 1% due to the experimental uncertainty on the corrected number of hadronic Z decays used for the normalization; 0.7% due to the uncertainty on the Higgs decay branching ratios; 2.4% on the Higgs detection efficiency due to limited Monte Carlo statistics.

Combining these errors in quadrature with the systematic error on the efficiency we obtain a total systematic uncertainty of 3.1% on the number of expected events for a 60 GeV Higgs signal, which has a small effect on the final result.

Intermediate mass $H^0\nu\bar{\nu}$ selection			
acollinearity	$<$	2.69	rad
θ_{123}	$<$	5.87	rad
$y_B^{\perp}$	$<$	0.646	
$\not{E}_{25}$	$<$	0.74	GeV
$\not{E}_{25}^{\perp}$	$<$	7.83	GeV
$P_{\perp}$	$>$	9.14	GeV
$P_{\perp}/E_{\text{vis}}$	$>$	0.344	
$\lvert P_{\parallel}\rvert/E_{\text{vis}}$	$<$	0.6	
E_{vis}	$<$	53.8	GeV
$\sin(\theta_{miss})$	$>$	0.503	
$\min(\sin(\theta_{\text{jet1}}), \sin(\theta_{\text{jet2}}))$	$>$	0.4	
$\min(E_{jet1}, E_{jet2})/E_{\text{vis}}$	$>$	0.25	
α^G	$<$	2.67	rad

Table 3: Values of the cuts for the $15 \div 50$ GeV mass $H^0\nu\bar{\nu}$ selection determined with the optimization procedure described in the text.

3.5 Mass Range 15 GeV $< M_H <$ 50 GeV

The analysis in this mass region is performed in a similar way as in the high mass range. Signal events, due to the large amount of missing momentum, are very unbalanced and this feature permits a good separation from hadronic Z decays. Two photon interactions with hadronic final states are rejected by requiring large visible energy and large total transverse momentum.

We apply on the MC and data samples the same preselection described in section 3.4 except for modifications concerning the visible energy (10 GeV $< E_{\text{vis}} <$ 80 GeV) and the cut on $|P_{\parallel}|/E_{\text{vis}}$ which is relaxed due to the higher momentum imbalance expected for this mass range. Applying the same procedure as for the high mass case we optimize the efficiency for a 30 GeV Higgs and we obtain the cut values given in Table 3.

The efficiencies for this selection are quoted in Table 2. The systematic errors are evaluated in the same way as for the high mass selection.

We find no candidates in the data collected from 1991 to 1994. The expected background is 0.07 events from $q\bar{q}$ and two photon interactions and 0.03 events from $\tau^+\tau^- b\bar{b}$ and $\nu\bar{\nu}q\bar{q}$.

3.6 Mass Range $M_H <$ 15 GeV

The signature of the signal in this mass range is a monojet coming from the decay of the H^0 and the absence of any activity in the opposite region of the detector.

The main backgrounds are due to two photon interactions, when the detected particles have high total transverse momentum, and to $\tau^+\tau^-$ events when a neutrino, coming from the decay of the τ, takes almost the entire available momentum.

It should be noticed that for M_H smaller than $2m_\mu$ the Higgs boson lifetime is very long. This implies that most of the times the Higgs decay occurs outside the TEC (50 cm of radius) producing events without charged tracks.

The selection is based on the following criteria: presence of a single jet, rejection of $\gamma\gamma$ interaction events with an electron observed in the luminosity monitor or in the lead–scintillator ring calorimeter and requirement of large transverse momentum.

The visible energy of the event is required to be below 60 GeV. To exploit the monojet topology of the signal one jet must have at least two good tracks and at least 5 GeV of energy while in the opposite hemisphere we require absence of charged tracks and an energy of at most 3 GeV. In case of two reconstructed jets the angle between them must be less than 2.8 rad both in space and in the plane perpendicular to the beam axis. In addition we require $\not{E}^{\perp}_{25} = 0$.

To reject $\tau^+\tau^-$background (three prong decay on one side and a very low energy electron on the other side) we require the number of good tracks belonging to the monojet to be different from three.

Events coming from $\gamma\gamma$ interactions are rejected by tagging the electrons in the very forward region of the detector. The events must have less than 3 GeV deposited in the luminosity monitor and less than 0.3 GeV in the ALR, the transverse momentum must be greater than 7 GeV and the polar angle of the total momentum must be at least 40° away from the beam axis.

The calculation of the signal efficiency in this mass range largely depends on the quality of the Monte Carlo simulation for the trigger, TEC, ALR and the luminosity monitor. Various cross checks with the data are performed in order to assure the validity of the simulation and to estimate the related systematic uncertainties.

Using the redundancy of the different triggers for the signal we calculate the effect of trigger efficiency from a data sample with similar topological features. The trigger efficiency is computed as a function of the calorimetric energy released in the detector and is then used to weight Monte Carlo events. The efficiency loss due to the trigger is significant for Higgs masses below 5 GeV.

The single track inefficiency in the polar angle region $33° < \theta < 147°$ is estimated to be 3.4% using the Monte Carlo $q\bar{q}$ events and 6.1% using three prong τ decays in the data. The signal efficiency is corrected for this difference. The efficiency correction factor ranges from –5.4% at $M_H = 0.1$ GeV to –0.5% at $M_H = 15$ GeV (see Table 4).

The noise in the small angle detectors, ALR and the luminosity monitor, derived from the study of randomly triggered events in coincidence with the beam crossing, is responsible for a relative loss of efficiency of 1.1%.

Corrected signal efficiencies for the low mass search are shown in Table 4.

M_H (GeV)	0.1	0.3	0.5	2	5	9	15
$(\Delta\varepsilon/\varepsilon)_{TEC}$ (%)	–5.4	–5.4	–5.4	–5.4	–3.4	–2.8	–0.5
ε (%)	3.0	14.8	13.2	20.1	26.3	28.6	29.6
$(\sigma_\varepsilon/\varepsilon)_{syst}$ (%)	15.4	15.4	15.4	15.4	10.3	9.0	8.6

Table 4: Correction factor due to TEC inefficiency, corrected efficiency and total systematic error as a function of M_H.

The uncertainties on the efficiency correction factors related to the ALR, the luminosity monitor and the TEC are estimated to be 50% of the correction factor itself. In addition the statistical error related to the trigger efficiency estimation is taken into account. All the other sources of systematic error are evaluated in the same way as described before. The combined systematic uncertainty is shown in Table 4 for each mass point.

For the low mass search we have analysed the data collected by L3 from 1992 to 1994, equivalent to 2.74 million hadronic Z decays. In this mass range we do not include the 1991 data because the ALR was not yet installed and this detector is essential to veto $\gamma\gamma$ interactions.

We estimate background contributions of 1.0 ± 1.0 events from $\gamma\gamma \to \mathrm{e^+e^-}\mu^+\mu^-$ and 0.11 ± 0.03 events from $\nu\bar{\nu}\mathrm{f}\bar{\mathrm{f}}$. All other sources of background investigated are found to be negligible.

We find one candidate in the data sample (from 1994) which has an invariant mass of 3.9 ± 2.4 GeV, a total transverse momentum of 7.06 GeV and a missing mass of 82.8 ± 3 GeV. This event is consistent with the expected two photon background.

4 $\mathrm{H^0e^+e^-}$ Channel

4.1 Mass Range 30 GeV $< M_H <$ 70 GeV

The signature of this process is the presence of two energetic and well separated electrons coming from the virtual Z^*, isolated from the H^0 decay products. The main sources of background are the four-fermion process $\mathrm{e^+e^-} \to \mathrm{e^+e^-q\bar{q}}$ and the double semileptonic decay $\mathrm{Z} \to \mathrm{b\bar{b}} \to \mathrm{e^+e^-}X$.

Low multiplicity events, such as $\mathrm{e^+e^-}$ and $\tau^+\tau^-$ final states, are removed by requiring at least 16 clusters in the electromagnetic calorimeter. To reduce the hadronic background we require that the two most energetic clusters have energies greater than 3 GeV and that the sum of their energies exceeds 15 GeV; in addition the angle between these two clusters must be larger than 40°.

The identification of electromagnetic particles is mainly based on the energy deposition pattern in the electromagnetic calorimeter. We use the ratio of the energies deposited in a 3×3 and in a 5×5 crystal array both centred on the most energetic crystal in the cluster as described in Reference [8]. The isolation of the electron candidate is ensured by imposing conditions on the energy deposited in the electromagnetic and hadronic calorimeters between two cones of 5° and 15° half opening angle around the BGO cluster direction. To complete the identification of the electrons we consider all pairs out of the three most energetic electron candidates. We accept the event if there is at least one pair with the most energetic cluster matching in azimuthal angle, within a 4σ cut, with exactly one track and the second most energetic cluster with at least one track. If the two selected electrons have an energy lower than 18 GeV each, they must also have opposite reconstructed charges.

To identify the Higgs boson decay products we examine the hadronic jets in the event. Indicating with $\mathrm{P}_\perp$ the transverse momentum of each electron with respect to the nearest jet axis, we require the sum of the two $\mathrm{P}_\perp$ to be larger than 10 GeV, and the smallest one to be at least 1 GeV. In the $\mathrm{H^0e^+e^-}$ and $\mathrm{H}^0\mu^+\mu^-$ analyses jets are formed using the jet algorithm described in Reference [25].

To reject the background from the four fermion processes we require that $2M_{\mathrm{e^+e^-}} + M_{\mathrm{recoil}}$ exceeds 80 GeV where $M_{\mathrm{e^+e^-}}$ is the invariant mass of the electron pair and M_{recoil} is the recoil mass against the two electrons.

The selection efficiencies for the signal are shown in Table 2. The relative systematic error on the signal efficiency, mainly due to the lepton isolation criteria, is always below 3.0%. The systematic error due to the limited Monte Carlo statistics is 1.5% for a 60 GeV Higgs boson. All other sources of systematic uncertainty on the number of expected signal events have already been described in the $\mathrm{H}^0\nu\bar{\nu}$ section.

Two events pass the above selection criteria. The first one, with a recoil mass against the two electrons of 31.4 ± 1.5 GeV, is from the 1991 data sample; the second one, from the 1992 data sample, has a recoil mass of 67.6 ± 0.7 GeV. The main parameters of these events have already been reported [8, 26].

The observed events are consistent with the expected background from $e^+e^- \rightarrow e^+e^-q\bar{q}$ processes. We expect 3.0$\pm$0.7 events for a recoil mass greater than 30 GeV estimated using the FERMISV program. Less than one $Z \rightarrow q\bar{q}$ event with recoil mass greater than 30 GeV is expected. The background from other processes is negligible. Figure 3-a shows the recoil mass distribution for the expected background and data.

4.2 Mass Range 4 GeV $< M_H <$ 30 GeV

The analysis in this mass range is performed following the same criteria as in the high mass search, with modifications so as to take into account the different kinematics. In fact the leptons here have more energy than the hadronic system.

In order to reject e^+e^- and $\tau^+\tau^-$ pairs, we require at least 6 clusters in the BGO electromagnetic calorimeter and more than two tracks in the TEC. The acoplanarity angle of the two electrons must be smaller than 179°. If the number of clusters in the BGO is lower than 11, we require the number of jets to be greater than 2 and the acoplanarity to be smaller than 175°. The event is also rejected if the third most energetic cluster is an electromagnetic one with an energy greater than 3 GeV or if it matches with two TEC tracks. The latter condition removes photon conversions with two close electrons.

To remove hadronic background, we select events with less than 50 clusters in the BGO, with the sum of the energy of the two most energetic isolated electromagnetic clusters larger than 26 GeV. The selection of isolated electromagnetic particles, their identification as electrons and TEC matching are based on the same criteria as in the high-mass range.

For the isolation of the electrons with respect to the hadronic jets we require the sum of the two $P_\perp$ to be greater than 15 GeV and the lowest $P_\perp$ to be greater than 1 GeV. To remove four-fermion events we apply the same criteria as for the high mass range.

The Higgs boson selection efficiencies are shown in Table 2. The systematic uncertainties have already been described in the high mass section. Nineteen data events pass the above selection criteria. These events are consistent with the 22.6 $\pm$ 1.5 expected events from four-fermion background and less than one expected from $\tau^+\tau^-$ background.

4.3 Mass Range $M_H <$ 4 GeV

We search for a low mass Higgs boson decaying into electrons, muons or hadrons. The main background sources are the four fermion processes and radiative Bhabha events with a photon converting in the beam pipe or in the material of TEC. Due to the long lifetime of the Higgs boson, for masses below $2m_\mu$, an event is expected to contain only two acoplanar electrons coming from the Z^* with no other detected particles balancing the missing momentum. The background for such events is mainly due to $\tau^+\tau^-$ and radiative Bhabha events, with the photon escaping detection.

In order to remove high multiplicity events we require at most 6 TEC tracks, 14 clusters in the BGO and 5 clusters in the hadronic calorimeter. The identification of the electron pair, from the Z^* decay, is performed as explained before with the additional requirement that the total energy of the two most energetic electromagnetic clusters be more than 30 GeV. Then we require electron isolation asking for less than 3 GeV in the BGO, excluding the electron energy, in a cone of 30° half opening angle around the electron direction and we require the direction recoiling against the two electrons to be away from the beam pipe by more than 15°.

Depending on the Higgs lifetime we may have different signal event topologies. The Higgs can decay inside or outside the TEC and even outside the detector.

To cover the main topologies three different selections have been used. The first one selects events with only two electron tracks, with the acoplanarity angle of the two electrons larger than 0.05 radian and with no or more than two neutral electromagnetic clusters ($e^+e^-(n\gamma)$ rejection). The second one selects events which, besides the electrons, have at least one track in the muon chambers. The third one selects events with the Higgs decaying inside the TEC. To recognize this decay the sum of the energies of the hadronic and electromagnetic clusters has to be greater than 1 GeV in the cone of 30° half opening angle around the missing momentum direction. In addition at least one charged track must be inside this cone. Radiative Bhabha events with γ conversion are removed by defining a γ conversion as a single cluster associated with 2 tracks.

We have performed several Monte Carlo simulations with the Higgs boson decaying into pairs of e, μ, π, K at various masses in the range $M_H < 4$ GeV. The corresponding selection efficiencies are given in Table 5. For Higgs hadronic decays in the mass range $2 \cdot m_\pi < M_H < 2$ GeV there are large uncertainties in the branching ratios. Based on isospin considerations we estimate an overall signal efficiency of 9%, as a weighted average of the efficiencies for neutral and charged hadrons.

Higgs Mass (GeV)	0.01	0.1	0.22	0.3	1.0	3.6
$H^0 \to e^+e^-$	8.2	7.4	–	–	13.6	–
$H^0 \to \mu^+\mu^-$	–	–	22.0	–	28.0	24.0
$H^0 \to \pi^+\pi^-$	–	–	–	9.4	17.0	15.0
$H^0 \to K^+K^-$	–	–	–	–	13.0	16.0

Table 5: Selection efficiencies (in %) for a light Higgs boson in the $H^0e^+e^-$ channel, for the Higgs decaying into charged particles.

We find 35 events satisfying this selection, which has to be compared with the 26.9 events expected from the background (21.2 four fermion events and 5.7 Bhabha events).

5 $H^0\mu^+\mu^-$ Channel

5.1 Mass Range 15 GeV $< M_H <$ 70 GeV

The main background processes for this channel are hadronic events with two semileptonic decays and four fermion events $e^+e^- \to \mu^+\mu^- q\bar{q}$. Muons from hadronic Z decays are usually included in the jets associated with the parton having the semileptonic decay. Isolation criteria can reduce this background. Four fermion processes, especially $e^+e^- \to Z \to q\bar{q}\gamma^* \to q\bar{q}\mu^+\mu^-$, where the muon pair tends to have a low invariant mass, constitute an irreducible background for this channel.

We require two muon tracks in the event with a distance of closest approach of each extrapolated track to the interaction point smaller than 3.5 standard deviations in both the z and the $R - \phi$ projections. To eliminate low charged multiplicity backgrounds, such as $\mu^+\mu^-e^+e^-$ and $\mu^+\mu^-\pi^+\pi^-$, we require more than four tracks and at least 8 calorimetric clusters. A first reduction of both hadronic and four fermion background is obtained requiring the thrust of the event to be smaller than 0.92 and the sum of the two muon momenta, $p_1 + p_2$, to be greater than 20 GeV, where both p_1 and p_2 must be larger than 3.4 GeV.

The final selection concerns the definition of isolation variables for the muons. For each muon we define: $\mathcal{D} = (E_{jet} - p_\mu)/p_\mu$ where p_μ is the muon momentum and E_{jet} is the energy of the jet containing the muon. We consider two cones of 15° and 3° half opening angles with their axes along the direction of the muon and we compute $E^{bgo}_{15^\circ}$ and $E^{bgo}_{3^\circ}$ as the electromagnetic energy in these cones, the latter being essentially from the muon, and we define: $\mathcal{E}^{bgo} = E^{bgo}_{15^\circ} - E^{bgo}_{3^\circ}$. In a similar way we define $\mathcal{E}^{hcl} = E^{hcl}_{30^\circ} - E^{hcl}_{3^\circ}$ in the hadronic calorimeter.

The three variables $\mathcal{D}$, $\mathcal{E}^{bgo}$ and $\mathcal{E}^{hcl}$ have a good rejection power, especially if the correlation between the two sets of variables corresponding to the two muons is taken into account. Two–dimensional cuts on those variables are applied which reject all the events in the $\mathrm{q\bar{q}}$ sample and substantially reduce the four fermion background. The analysis has been optimized for a Higgs mass of 60 GeV. The values of the cuts are the following: $\mathcal{D}_{1,2} < 2.5$, $\mathcal{D}_1 \cdot \mathcal{D}_2 < 0.25$; $\min(\mathcal{E}^{bgo}_1, \mathcal{E}^{bgo}_2) < 200$ MeV; $\mathcal{E}^{hcl}_{1,2} < 4$ GeV, $\mathcal{E}^{hcl}_1 \cdot \mathcal{E}^{hcl}_2 < 1$ GeV^2, where the index refers to the muon candidate.

Selection efficiencies are presented in Table 2. The systematic error on the signal efficiency is 6.5%. The other sources of systematic error on the number of expected signal events have already been described in the $\mathrm{H}^0\nu\bar{\nu}$ analysis. No events pass the selection criteria in the data sample collected from 1991 to 1994 while the background expected from $\mathrm{e^+e^-} \to \mu^+\mu^-\mathrm{q\bar{q}}$ is 0.65 ± 0.11 events for a recoil mass greater than 30 GeV; other sources of background give negligible contributions.

5.2 Mass Range 2 GeV $< M_H <$ 15 GeV

The first requirements for the two muons are the same as for the high mass search. In order to eliminate very low charged multiplicity backgrounds more than 2 tracks and at least 7 calorimetric clusters are required. On the other hand the high multiplicity hadronic background is reduced by requiring a maximum of 10 tracks.

A cut of $p_1 + p_2 > 30$ GeV is applied, and to reduce the four fermion background with the hadronic system coming from the radiated photon, we require $\max(p_1, p_2) < 43$ GeV. To better define the kinematical region of interest we ask the invariant mass of the muon system to be greater than 15 GeV and the recoil mass, with respect to the muon system, to be less than 25 GeV. Finally we apply two isolation cuts for the muon with respect to the hadronic system: $\min(\mathcal{D}_1, \mathcal{D}_2) < 0.3$ and $\min(\mathcal{E}^{bgo}_1, \mathcal{E}^{bgo}_2) < 250$ MeV.

Selection efficiencies are shown in Table 2 and their systematic errors are the same as those for the high mass selection. The expected background from $\mathrm{e^+e^-} \to \mu^+\mu^-\mathrm{q\bar{q}}$ is 1.9 ± 0.2 events; other sources of background give negligible contributions. Two events are found in the data sample collected from 1991 to 1994, one from the 1992 data with a recoil mass against the muons of 5.3 ± 1.0 GeV and one from the 1993 data with a recoil mass of 9.6 ± 1.0 GeV. The spectrum of the $\mu^+\mu^-$ recoil mass expected from the four fermion background is shown in Figure 3-b together with the two candidates.

6 Results

6.1 Standard Model High Mass Higgs

No evidence for a signal appears in this search. No high mass events are observed in the $H^0\nu\bar{\nu}$ and $H^0\mu^+\mu^-$ channels. The candidates observed in the $H^0e^+e^-$ channel, taking into account the mass resolution, are not consistent with a Higgs mass of 60 GeV. Thus a 95% C.L. limit is set at a mass value where the number of expected events is 3. The number of expected events has been calculated using a $\tau^+\tau^-$ branching ratio for a 60 GeV Higgs boson of 9.0% and has been reduced by one standard deviation of the systematic error.

Higgs mass (GeV)	50	55	60	65	70
$H^0\nu\bar{\nu}$ channel	11.30	5.30	2.17	0.553	0.113
$H^0e^+e^-$ channel	2.50	1.27	0.57	0.228	0.072
$H^0\mu^+\mu^-$ channel	1.88	0.92	0.42	0.145	0.006

Table 6: Number of expected Higgs events in the different channels for the high mass search after subtracting one standard deviation of the systematic error.

We report in Table 2 the efficiencies and in Table 6 the number of expected events in the vicinity of the limit, reduced by one standard deviation of the systematic error, for all the channels. In Figure 4 we show the number of Higgs events expected in the different channels as a function of the Higgs mass together with the 95% confidence level line and with the corresponding Higgs mass limit.

We obtain a lower limit for the SM Higgs boson mass of:

$$M_H > 60.2 \text{ GeV at } 95\% \text{ C.L.}$$

6.2 Neutral Two Doublet Model Higgs

The search for the Higgs boson has been extended for masses smaller than 50 GeV, because the production rate in Two Doublet Models can be suppressed with respect to the Standard Model. Below 50 GeV we have used the combination in logical OR of the analyses for the different mass ranges. The efficiencies for the different channels are quoted in Tables 2, 4 and 5. The drop in efficiency in the $h^0\nu\bar{\nu}$ channel for M_{h^0} below $2m_\mu$ (Table 4) is due to the long lifetime of the Higgs boson, in which case the Higgs decays outside the TEC and the event does not have the charged tracks required by the selection. The reduced statistics (without 1991 data) of the $H^0\nu\bar{\nu}$ low mass search is taken into account by reducing the efficiency for the low mass range when combining with the other analyses.

No evidence for a signal has been observed. In the three channels that have been studied the observed candidates are consistent with the expected background. From this negative result limits are obtained in the framework of non minimal Higgs models.

Figure 5-a shows the number of expected events, reduced by one standard deviation of the systematic error, as a function of the Higgs mass. Figure 5-b shows the 95% C.L. upper limit that we obtain on the ratio between the cross section of the bremsstrahlung production of the Higgs boson in the Two Doublet Model and that of the SM Higgs boson, assuming that the non minimal Higgs boson has the same decay branching ratios. For Higgs masses below 100 MeV

the $h^0\nu\bar{\nu}$ channel does not contribute any more and the sensitivity comes only from the charged leptonic channels. For $M_{h^0} < 100$ MeV the number of expected signal events is equal to 100 and we set an upper limit of 0.1 on the ratio between the cross section of the bremsstrahlung production of the Higgs boson in the Two Doublet Model and that in the Standard Model.

6.3 Invisible Higgs Decays

If we consider a non minimal Higgs boson (h^{inv}) which decays into a final state invisible to the detector, produced in association with a Z^* which decays into a $q\bar{q}$ pair, the signature is very similar to that of the $H^0\nu\bar{\nu}$ channel. The previous analysis for $H^0\nu\bar{\nu}$ channel which selects only one candidate consistent with the expected background is therefore valid also for this channel and an upper limit can be derived for the production cross section as function of the invisible Higgs boson mass.

$M_{h^{inv}}$ (GeV)	0.1	5	10	20	30	40	50	60	70
ε (%)	6.8	12.8	18.5	30.1	39.4	39.6	39.5	37.9	32.5

Table 7: Selection efficiencies for the process $e^+e^- \to h^{inv}q\bar{q}$.

Table 7 shows the efficiencies for the process $e^+e^- \to h^{inv}q\bar{q}$. The $h^0\nu\bar{\nu}$ low mass selection is also efficient (about 15% for $M_{h^{inv}} = 60$ GeV) for Higgs invisible decays in association with Z^* leptonic decays ($h^{inv}\ell^+\ell^-$). This small additional sensitivity is taken into account when calculating the limit. The reduced statistics (without 1991 data) of the $h^0\nu\bar{\nu}$ low mass search is converted into a reduced efficiency for the low mass range when combined with the other two $h^0\nu\bar{\nu}$ analyses. Figure 6-a shows the number of expected events, reduced by one standard deviation of the systematic error, and the Higgs mass limit at the 95% C.L. Figure 6-b shows the 95% C.L. upper limit that we obtain on the ratio between the cross section of the bremsstrahlung production of the non minimal Higgs boson with an invisible decay and that of the SM Higgs boson. The candidate selected by our selection is outside the mass range under consideration ($M_{h^{inv}} = 82.8 \pm 3$ GeV) and therefore the 95% C.L. line is set at 3 events expected.

Assuming that the cross section is the same as for the SM Higgs boson we obtain a lower limit for the mass of h^{inv} of:

$$M_{h^{inv}} > 66.7 \text{ GeV at 95\% C.L.}$$

7 Conclusions

We search for the neutral Standard Model Higgs boson, produced through $e^+e^- \to Z^*\,H^0$, using data collected by the L3 detector from 1991 to 1994, equivalent to about 3.05 M hadronic Z decays, at LEP e^+e^- collider. Three decay channels of the virtual Z are analysed: $H^0e^+e^-$, $H^0\mu^+\mu^-$ and $H^0\nu\bar{\nu}$. We find no evidence for a signal in the mass range covered and we set a 95% C.L. lower limit on the mass of the Standard Model Higgs boson of 60.2 GeV. These searches are also interpreted in the framework of the General Two Doublet Model and we set an upper limit on the ratio between the cross section of the bremsstrahlung production of a non minimal Higgs boson and that of the SM Higgs boson. Invisible decays of the Higgs boson are considered and we derive a 95% C.L. lower limit on the mass of the Higgs boson of 66.7 GeV for a production cross section equal to that of the Standard Model.

Acknowledgements

We wish to express our gratitude to the CERN accelerator divisions for the excellent performance of the LEP machine. We acknowledge the contributions of all the engineers and technicians who have participated in the construction and maintenance of this experiment. Those of us who are not from member states thank CERN for its hospitality and help.

References

[1] S. L. Glashow, Nucl. Phys. **22** (1961) 579;
S. Weinberg, Phys. Rev. Lett. **19** (1967) 1264;
A. Salam, "Elementary Particle Theory", ed. N. Svartholm, Stockholm, "Almquist and Wiksell" (1968), 367.

[2] P. W. Higgs, Phys. Lett. **12** (1964) 132, Phys. Rev. Lett. **13** (1964) 508 and Phys. Rev. **145** (1966) 1156;
F. Englert and R. Brout, Phys. Rev. Lett. **13** (1964) 321.

[3] J. D. Bjorken in "Proceedings of Summer Institute on Particle Physics, August 2-13 1976. Weak Interactions at High Energy and the production of New Particles", SLAC Report 198, Ed. M. C. Zipf, (Stanford Linear Accel. Center, Stanford, 1976), and "Weak Interaction Theory and Neutral Currents", SLAC-PUB-1866 (1977) 1;
B.L. Ioffe and V.A. Khoze, Sov. J. Part. Nucl. **9** (1978) 50;
J. Finjord, Phys. Scripta **21** (1980) 143.

[4] E. Gross, B. A. Kniehl and G. Wolf, Z. Phys. **C 63** (1994) 417;
erratum-ibid- **C 66** (1995) 321.

[5] B. A. Kniehl, Phys. Lett. **B 282** (1992) 249.

[6] H. P. Nilles, Phys. Rep. **110** (1984) 1;
H. E. Haber and G. L. Kane, Phys. Rep. **117** (1985) 75;
R. Barbieri, Nuovo Cimento **11** no.4 (1988) 1.

[7] A. Lopez-Fernandez *et al.*, Phys. Lett. **B 312** (1993) 240;
F. De Campos *et al.*, Phys. Lett. **B 336** (1994) 446;
A. Djouadi *et al.*, CERN preprint CERN-PPE/96-34.

[8] L3 Collaboration, O. Adriani *et al.*, Phys. Lett. **B303** (1993) 391;
L3 Collaboration, O. Adriani *et al.*, Z. Phys. **C57** (1993) 355.

[9] ALEPH Collaboration, D. Buskulic *et al.*, Phys. Lett. **B313** (1993) 299;
ALEPH Collaboration, D. Buskulic *et al.*, Phys. Lett. **B313** (1993) 312.

[10] OPAL Collaboration, R. Akers *et al.*, Phys. Lett. **B327** (1994) 397;
OPAL Collaboration, R. Akers *et al.*, Z. Phys. **C64** (1994) 1.

[11] DELPHI Collaboration, P. Abreu *et al.*, Nucl. Phys. **B421** (1994) 3;
DELPHI Collaboration, P. Abreu *et al.*, Z. Phys. **C67** (1995) 69.

[12] L3 Collab., B. Adeva *et al.*, Nucl. Inst. Meth. **A 289** (1990) 35.

[13] M. Acciarri *et al.*, Nucl. Inst. Meth. **A 351** (1994) 300.

[14] M. Chemarin *et al.*, Nucl. Inst. Meth. **A 349** (1994) 345.

[15] M. Merk, Proceedings of the XXIXth Rencontre de Moriond, Meribel les Allues, France – March 12–19, 1994, p. 93, ed. J. Tran Thanh Van.

[16] The JETSET version 7.4 is used.
T. Sjöstrand, Comp. Phys. Comm. **39** (1986) 347;
T. Sjöstrand and M. Bengtsson, Comp. Phys. Comm. **43** (1987) 367.

[17] G. Marchesini and B.R. Webber, Nucl. Phys. **B 310** (1988) 461;
G. Marchesini *et al.*, Comp. Phys. Comm. **67** (1992) 465.

[18] F. A. Berends, P. H. Daverfeldt and R. Kleiss, Nucl. Phys. **B 253** (1985) 441.

[19] J.A.M. Vermaseren, Nucl. Phys. **B 229** (1983) 347.

[20] The KORALZ version 4.01 is used.
S. Jadach, B. F. L. Ward and Z. Wąs, Comp. Phys. Comm. **79** (1994) 503.

[21] J. H. Field, Phys. Lett. **B 323** (1994) 432;
J. H. Field and T. Riemann, Preprints UGVA–DPNC 1995/6–166 and DESY 95–100, to be published in Comp. Phys. Comm.

[22] J. Hilgart, R. Kleiss and F. Le Diberder, Comp. Phys. Comm. **73** (1993) 191.

[23] A. Favara and M. Pieri, L3 Internal Note 1728, March 1995 [1)].

[24] F. James, CERN Program Library Long Writeup D506 MINUIT, CERN, 1993.

[25] O. Adriani *et al.*, Nucl. Inst. Meth. **A 302** (1991) 53.

[26] L3 Collaboration, B. Adeva *et al.*, Phys. Lett. **B283** (1992) 454.

[1)]These L3 Internal Notes are freely available on request from: The L3 secretariat, CERN, CH–1211 Geneva 23, Switzerland. Internet: http://hpl3sn02.cern.ch/l3pubanddoc.html

The L3 Collaboration:

M.Acciarri,[28] O.Adriani,[17] M.Aguilar-Benitez,[27] S.Ahlen,[11] B.Alpat,[35] J.Alcaraz,[27] G.Alemanni,[23] J.Allaby,[18]
A.Aloisio,[30] G.Alverson,[12] M.G.Alviggi,[30] G.Ambrosi,[20] H.Anderhub,[50] V.P.Andreev,[39] T.Angelescu,[13]
D.Antreasyan,[9] A.Arefiev,[29] T.Azemoon,[3] T.Aziz,[10] P.Bagnaia,[38] L.Baksay,[45] R.C.Ball,[3] S.Banerjee,[10] K.Banicz,[47]
R.Barillère,[18] L.Barone,[38] P.Bartalini,[35] A.Baschirotto,[28] M.Basile,[9] R.Battiston,[35] A.Bay,[23] F.Becattini,[17] U.Becker,[16]
F.Behner,[50] J.Berdugo,[27] P.Berges,[16] B.Bertucci,[18] B.L.Betev,[50] M.Biasini,[18] A.Biland,[50] G.M.Bilei,[35] J.J.Blaising,[18]
S.C.Blyth,[36] G.J.Bobbink,[2] R.Bock,[1] A.Böhm,[1] B.Borgia,[38] A.Boucham,[4] D.Bourilkov,[50] M.Bourquin,[20] D.Boutigny,[4]
E.Brambilla,[16] J.G.Branson,[41] V.Brigljevic,[50] I.C.Brock,[36] A.Buijs,[46] J.D.Burger,[16] W.J.Burger,[20] J.Busenitz,[45]
A.Buytenhuijs,[32] X.D.Cai,[19] M.Campanelli,[50] M.Capell,[16] G.Cara Romeo,[9] M.Caria,[35] G.Carlino,[4] A.M.Cartacci,[17]
J.Casaus,[27] G.Castellini,[17] R.Castello,[28] F.Cavallari,[38] N.Cavallo,[30] C.Cecchi,[20] M.Cerrada,[27] F.Cesaroni,[24]
M.Chamizo,[27] A.Chan,[52] Y.H.Chang,[52] U.K.Chaturvedi,[19] M.Chemarin,[26] A.Chen,[52] G.Chen,[7] G.M.Chen,[7]
H.F.Chen,[21] H.S.Chen,[7] M.Chen,[16] G.Chiefari,[30] C.Y.Chien,[5] M.T.Choi,[44] L.Cifarelli,[40] F.Cindolo,[9] C.Civinini,[17]
I.Clare,[16] R.Clare,[16] H.O.Cohn,[33] G.Coignet,[4] A.P.Colijn,[2] N.Colino,[27] S.Costantini,[38] F.Cotorobai,[13] B.de la Cruz,[27]
A.Csilling,[14] T.S.Dai,[16] R.D'Alessandro,[17] R.de Asmundis,[30] H.De Boeck,[32] A.Degré,[4] K.Deiters,[48] P.Denes,[37]
F.DeNotaristefani,[38] D.DiBitonto,[45] M.Diemoz,[38] D.van Dierendonck,[2] F.Di Lodovico,[50] C.Dionisi,[38] M.Dittmar,[50]
A.Dominguez,[41] A.Doria,[30] I.Dorne,[4] M.T.Dova,[19,♯] E.Drago,[30] D.Duchesneau,[4] P.Duinker,[2] I.Duran,[42] S.Dutta,[10]
S.Easo,[35] Yu.Efremenko,[33] H.El Mamouni,[26] A.Engler,[36] F.J.Eppling,[16] F.C.Erné,[2] J.P.Ernenwein,[26] P.Extermann,[20]
M.Fabre,[48] R.Faccini,[38] S.Falciano,[38] A.Favara,[17] J.Fay,[26] O.Fedin,[39] M.Felcini,[50] T.Ferguson,[36] D.Fernandez,[27]
F.Ferroni,[38] H.Fesefeldt,[1] E.Fiandrini,[35] J.H.Field,[20] F.Filthaut,[36] P.H.Fisher,[16] G.Forconi,[16] L.Fredj,[20]
K.Freudenreich,[50] C.Furetta,[28] Yu.Galaktionov,[29,16] S.N.Ganguli,[10] S.S.Gau,[12] S.Gentile,[38] J.Gerald,[5]
N.Gheordanescu,[13] S.Giagu,[38] S.Goldfarb,[23] J.Goldstein,[11] Z.F.Gong,[21] A.Gougas,[5] G.Gratta,[34] M.W.Gruenewald,[8]
V.K.Gupta,[37] A.Gurtu,[10] L.J.Gutay,[47] K.Hangarter,[1] B.Hartmann,[1] A.Hasan,[31] T.Hebbeker,[8] A.Hervé,[18]
W.C.van Hoek,[32] H.Hofer,[50] H.Hoorani,[20] S.R.Hou,[52] G.Hu,[19] M.M.Ilyas,[19] V.Innocente,[18] H.Janssen,[4] B.N.Jin,[7]
L.W.Jones,[3] P.de Jong,[16] I.Josa-Mutuberria,[27] A.Kasser,[23] R.A.Khan,[19] Yu.Kamyshkov,[33] P.Kapinos,[49]
J.S.Kapustinsky,[25] Y.Karyotakis,[4] M.Kaur,[19,◇] M.N.Kienzle-Focacci,[20] D.Kim,[5] J.K.Kim,[44] S.C.Kim,[44] Y.G.Kim,[44]
W.W.Kinnison,[25] A.Kirkby,[34] D.Kirkby,[34] J.Kirkby,[18] D.Kiss,[14] W.Kittel,[32] A.Klimentov,[16,29] A.C.König,[32]
I.Korolko,[29] V.Koutsenko,[16,29] R.W.Kraemer,[36] T.Kramer,[16] W.Krenz,[1] H.Kuijten,[32] A.Kunin,[16,29]
P.Ladron de Guevara,[27] G.Landi,[17] C.Lapoint,[16] K.Lassila-Perini,[50] P.Laurikainen,[22] M.Lebeau,[18] A.Lebedev,[16]
P.Lebrun,[26] P.Lecomte,[50] P.Lecoq,[18] P.Le Coultre,[50] J.S.Lee,[44] K.Y.Lee,[44] C.Leggett,[3] J.M.Le Goff,[18] R.Leiste,[49]
M.Lenti,[17] E.Leonardi,[38] P.Levtchenko,[39] C.Li,[21] E.Lieb,[49] W.T.Lin,[52] F.L.Linde,[2,18] L.Lista,[30] Z.A.Liu,[7]
W.Lohmann,[49] E.Longo,[38] W.Lu,[34] Y.S.Lu,[7] K.Lübelsmeyer,[1] C.Luci,[38] D.Luckey,[16] L.Ludovici,[38] L.Luminari,[38]
W.Lustermann,[48] W.G.Ma,[21] A.Macchiolo,[17] M.Maity,[10] G.Majumder,[10] L.Malgeri,[38] A.Malinin,[29] C.Maña,[27]
S.Mangla,[10] P.Marchesini,[50] A.Marin,[11] J.P.Martin,[26] F.Marzano,[38] G.G.G.Massaro,[2] K.Mazumdar,[10] D.McNally,[18]
S.Mele,[30] L.Merola,[30] M.Meschini,[17] W.J.Metzger,[32] M.von der Mey,[1] Y.Mi,[23] A.Mihul,[13] A.J.W.van Mil,[32]
G.Mirabelli,[38] J.Mnich,[18] B.Monteleoni,[17] R.Moore,[3] S.Morganti,[38] R.Mount,[34] S.Müller,[1] F.Muheim,[20] E.Nagy,[14]
S.Nahn,[16] M.Napolitano,[30] F.Nessi-Tedaldi,[50] H.Newman,[34] A.Nippe,[1] H.Nowak,[49] G.Organtini,[38] R.Ostonen,[22]
D.Pandoulas,[1] S.Paoletti,[38] P.Paolucci,[30] H.K.Park,[36] G.Pascale,[38] G.Passaleva,[17] S.Patricelli,[30] T.Paul,[12]
M.Pauluzzi,[35] C.Paus,[1] F.Pauss,[50] D.Peach,[18] Y.J.Pei,[1] S.Pensotti,[28] D.Perret-Gallix,[4] S.Petrak,[8] A.Pevsner,[5]
D.Piccolo,[30] M.Pieri,[17] J.C.Pinto,[36] P.A.Piroué,[37] E.Pistolesi,[17] V.Plyaskin,[29] M.Pohl,[50] V.Pojidaev,[29,17] H.Postema,[16]
N.Produit,[20] D.Prokofiev,[39] R.Raghavan,[10] G.Rahal-Callot,[50] P.G.Rancoita,[28] M.Rattaggi,[28] G.Raven,[41]
P.Razis,[31] K.Read,[33] D.Ren,[50] M.Rescigno,[38] S.Reucroft,[12] T.van Rhee,[46] S.Riemann,[49] B.C.Riemers,[47] K.Riles,[3]
O.Rind,[3] S.Ro,[44] A.Robohm,[50] J.Rodin,[16] F.J.Rodriguez,[27] B.P.Roe,[3] S.Röhner,[1] L.Romero,[27] S.Rosier-Lees,[4]
Ph.Rosselet,[23] W.van Rossum,[46] S.Roth,[1] J.A.Rubio,[18] H.Rykaczewski,[50] J.Salicio,[18] E.Sanchez,[27] A.Santocchia,[35]
M.E.Sarakinos,[22] S.Sarkar,[10] M.Sassowsky,[1] G.Sauvage,[4] C.Schäfer,[1] V.Schegelsky,[39] S.Schmidt-Kaerst,[1] D.Schmitz,[1]
P.Schmitz,[1] M.Schneegans,[4] B.Schoeneich,[49] N.Scholz,[50] H.Schopper,[51] D.J.Schotanus,[32] J.Schwenke,[1] G.Schwering,[1]
C.Sciacca,[30] D.Sciarrino,[20] J.C.Sens,[52] L.Servoli,[35] S.Shevchenko,[34] N.Shivarov,[43] V.Shoutko,[29] J.Shukla,[25]
E.Shumilov,[29] A.Shvorob,[34] T.Siedenburg,[1] D.Son,[44] A.Sopczak,[49] V.Soulimov,[30] B.Smith,[16] P.Spillantini,[17]
M.Steuer,[16] D.P.Stickland,[37] F.Sticozzi,[16] H.Stone,[37] B.Stoyanov,[43] A.Straessner,[1] K.Strauch,[15] K.Sudhakar,[10]
G.Sultanov,[19] L.Z.Sun,[21] G.F.Susinno,[20] H.Suter,[50] J.D.Swain,[19] X.W.Tang,[7] L.Tauscher,[6] L.Taylor,[12]
Samuel C.C.Ting,[16] S.M.Ting,[16] F.Tonisch,[49] M.Tonutti,[1] S.C.Tonwar,[10] J.Tóth,[14] C.Tully,[37] H.Tuchscherer,[45]
K.L.Tung,[7] J.Ulbricht,[50] U.Uwer,[18] E.Valente,[38] R.T.Van de Walle,[32] G.Vesztergombi,[14] I.Vetlitsky,[29] G.Viertel,[50]
M.Vivargent,[4] R.Völkert,[49] H.Vogel,[36] H.Vogt,[49] I.Vorobiev,[29] A.A.Vorobyov,[39] A.Vorvolakos,[31] M.Wadhwa,[6]
W.Wallraff,[1] J.C.Wang,[16] X.L.Wang,[21] Y.F.Wang,[16] Z.M.Wang,[21] A.Weber,[1] F.Wittgenstein,[18] S.X.Wu,[19]
S.Wynhoff,[1] J.Xu,[11] Z.Z.Xu,[21] B.Z.Yang,[21] C.G.Yang,[7] X.Y.Yao,[7] J.B.Ye,[21] S.C.Yeh,[52] J.M.You,[36] An.Zalite,[39]
Yu.Zalite,[39] P.Zemp,[50] Y.Zeng,[1] Z.Zhang,[7] Z.P.Zhang,[21] B.Zhou,[11] Y.Zhou,[3] G.Y.Zhu,[7] R.Y.Zhu,[34] A.Zichichi.[9,18,19]

1 I. Physikalisches Institut, RWTH, D-52056 Aachen, FRG[§]
III. Physikalisches Institut, RWTH, D-52056 Aachen, FRG[§]
2 National Institute for High Energy Physics, NIKHEF, and University of Amsterdam, NL-1009 DB Amsterdam, The Netherlands
3 University of Michigan, Ann Arbor, MI 48109, USA
4 Laboratoire d'Annecy-le-Vieux de Physique des Particules, LAPP,IN2P3-CNRS, BP 110, F-74941 Annecy-le-Vieux CEDEX, France
5 Johns Hopkins University, Baltimore, MD 21218, USA
6 Institute of Physics, University of Basel, CH-4056 Basel, Switzerland
7 Institute of High Energy Physics, IHEP, 100039 Beijing, China[△]
8 Humboldt University, D-10099 Berlin, FRG[§]
9 INFN-Sezione di Bologna, I-40126 Bologna, Italy
10 Tata Institute of Fundamental Research, Bombay 400 005, India
11 Boston University, Boston, MA 02215, USA
12 Northeastern University, Boston, MA 02115, USA
13 Institute of Atomic Physics and University of Bucharest, R-76900 Bucharest, Romania
14 Central Research Institute for Physics of the Hungarian Academy of Sciences, H-1525 Budapest 114, Hungary[‡]
15 Harvard University, Cambridge, MA 02139, USA
16 Massachusetts Institute of Technology, Cambridge, MA 02139, USA
17 INFN Sezione di Firenze and University of Florence, I-50125 Florence, Italy
18 European Laboratory for Particle Physics, CERN, CH-1211 Geneva 23, Switzerland
19 World Laboratory, FBLJA Project, CH-1211 Geneva 23, Switzerland
20 University of Geneva, CH-1211 Geneva 4, Switzerland
21 Chinese University of Science and Technology, USTC, Hefei, Anhui 230 029, China[△]
22 SEFT, Research Institute for High Energy Physics, P.O. Box 9, SF-00014 Helsinki, Finland
23 University of Lausanne, CH-1015 Lausanne, Switzerland
24 INFN-Sezione di Lecce and Universitá Degli Studi di Lecce, I-73100 Lecce, Italy
25 Los Alamos National Laboratory, Los Alamos, NM 87544, USA
26 Institut de Physique Nucléaire de Lyon, IN2P3-CNRS,Université Claude Bernard, F-69622 Villeurbanne, France
27 Centro de Investigaciones Energeticas, Medioambientales y Tecnologicas, CIEMAT, E-28040 Madrid, Spain[♭]
28 INFN-Sezione di Milano, I-20133 Milan, Italy
29 Institute of Theoretical and Experimental Physics, ITEP, Moscow, Russia
30 INFN-Sezione di Napoli and University of Naples, I-80125 Naples, Italy
31 Department of Natural Sciences, University of Cyprus, Nicosia, Cyprus
32 University of Nymegen and NIKHEF, NL-6525 ED Nymegen, The Netherlands
33 Oak Ridge National Laboratory, Oak Ridge, TN 37831, USA
34 California Institute of Technology, Pasadena, CA 91125, USA
35 INFN-Sezione di Perugia and Universitá Degli Studi di Perugia, I-06100 Perugia, Italy
36 Carnegie Mellon University, Pittsburgh, PA 15213, USA
37 Princeton University, Princeton, NJ 08544, USA
38 INFN-Sezione di Roma and University of Rome, "La Sapienza", I-00185 Rome, Italy
39 Nuclear Physics Institute, St. Petersburg, Russia
40 University and INFN, Salerno, I-84100 Salerno, Italy
41 University of California, San Diego, CA 92093, USA
42 Dept. de Fisica de Particulas Elementales, Univ. de Santiago, E-15706 Santiago de Compostela, Spain
43 Bulgarian Academy of Sciences, Central Laboratory of Mechatronics and Instrumentation, BU-1113 Sofia, Bulgaria
44 Center for High Energy Physics, Korea Advanced Inst. of Sciences and Technology, 305-701 Taejon, Republic of Korea
45 University of Alabama, Tuscaloosa, AL 35486, USA
46 Utrecht University and NIKHEF, NL-3584 CB Utrecht, The Netherlands
47 Purdue University, West Lafayette, IN 47907, USA
48 Paul Scherrer Institut, PSI, CH-5232 Villigen, Switzerland
49 DESY-Institut für Hochenergiephysik, D-15738 Zeuthen, FRG
50 Eidgenössische Technische Hochschule, ETH Zürich, CH-8093 Zürich, Switzerland
51 University of Hamburg, D-22761 Hamburg, FRG
52 High Energy Physics Group, Taiwan, China
§ Supported by the German Bundesministerium für Bildung, Wissenschaft, Forschung und Technologie
‡ Supported by the Hungarian OTKA fund under contract number T14459.
♭ Supported also by the Comisión Interministerial de Ciencia y Technología
♯ Also supported by CONICET and Universidad Nacional de La Plata, CC 67, 1900 La Plata, Argentina
◇ Also supported by Panjab University, Chandigarh-160014, India
△ Supported by the National Natural Science Foundation of China.

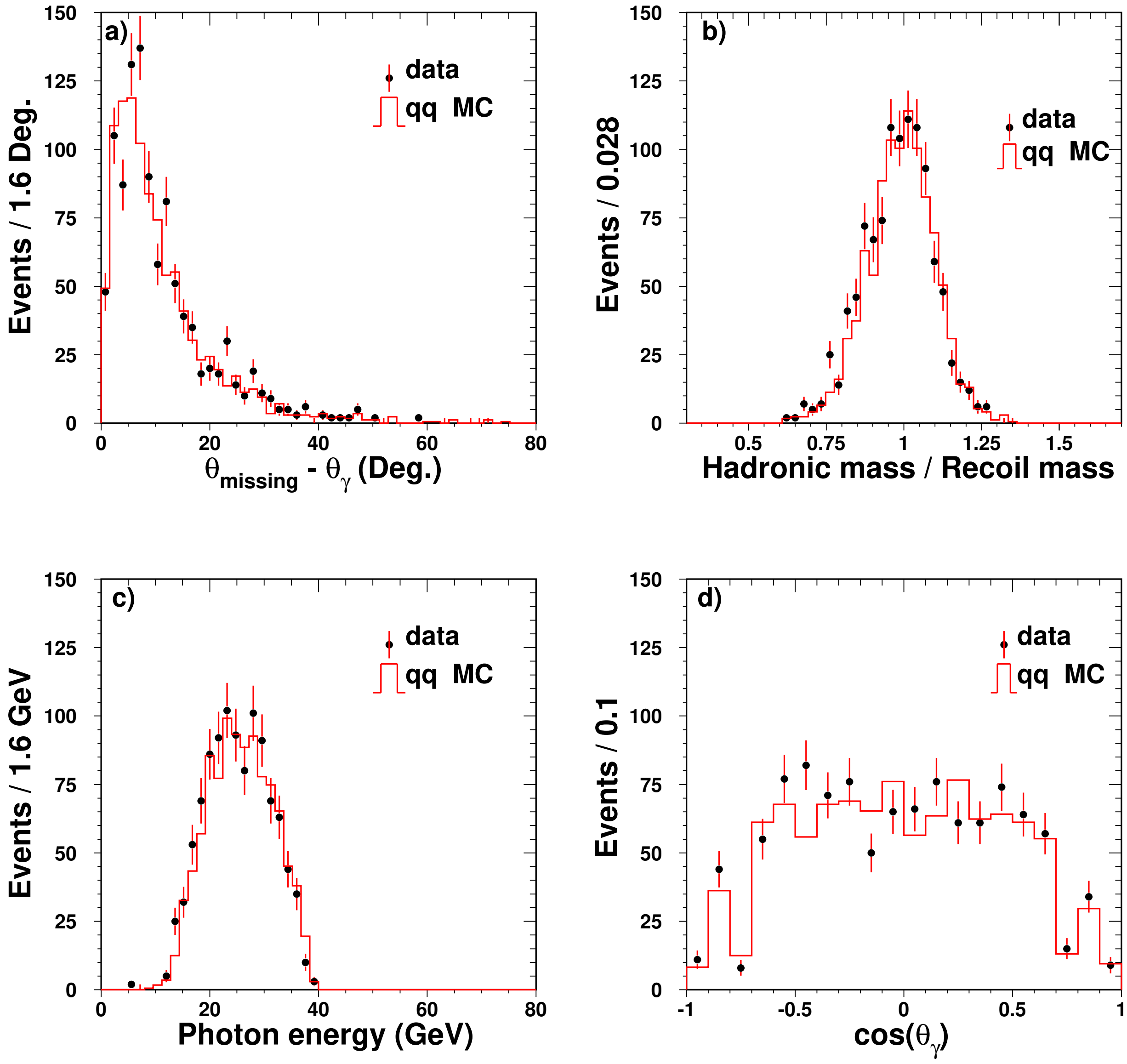

Figure 1: Comparisons between data (dots) and Monte Carlo (histogram) for the selected $q\bar{q}\gamma$ events. a) the distribution of the angle between the photon and the missing momentum directions obtained when ignoring the photon in the reconstruction; b) the distribution of the ratio between the mass computed from the hadronic system and the mass recoiling to the photon; c) and d) the distributions of the energy and of the polar angle of the radiated photon.

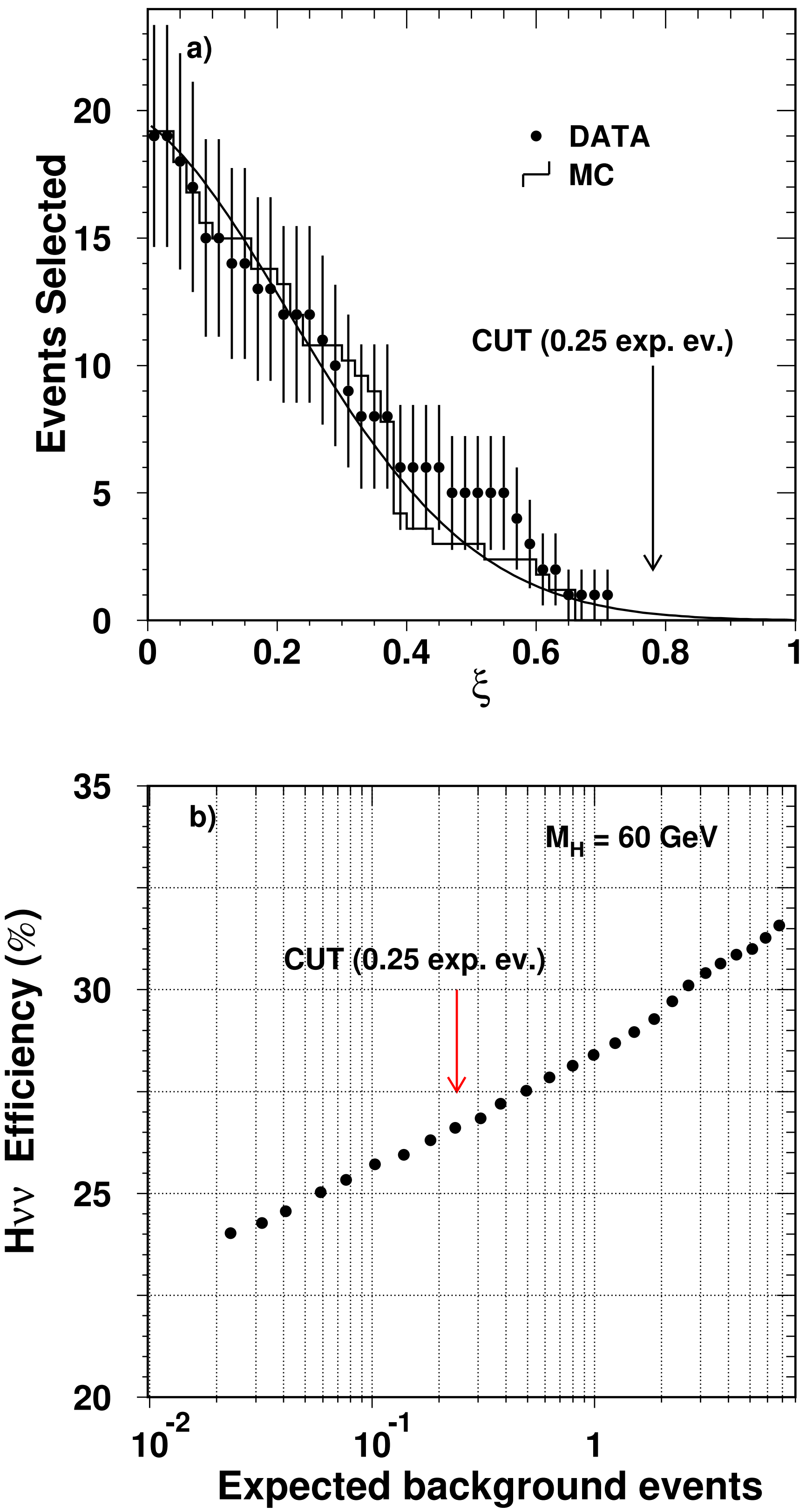

Figure 2: a) Number of events selected as a function of the cut variable ξ in the $H^0\nu\bar{\nu}$ channel. The solid line shows the Gaussian fit to the Monte Carlo distribution, the arrow indicates the position of the final cut on the variable ξ. b) Signal efficiency for $M_H = 60$ GeV versus number of expected background events.

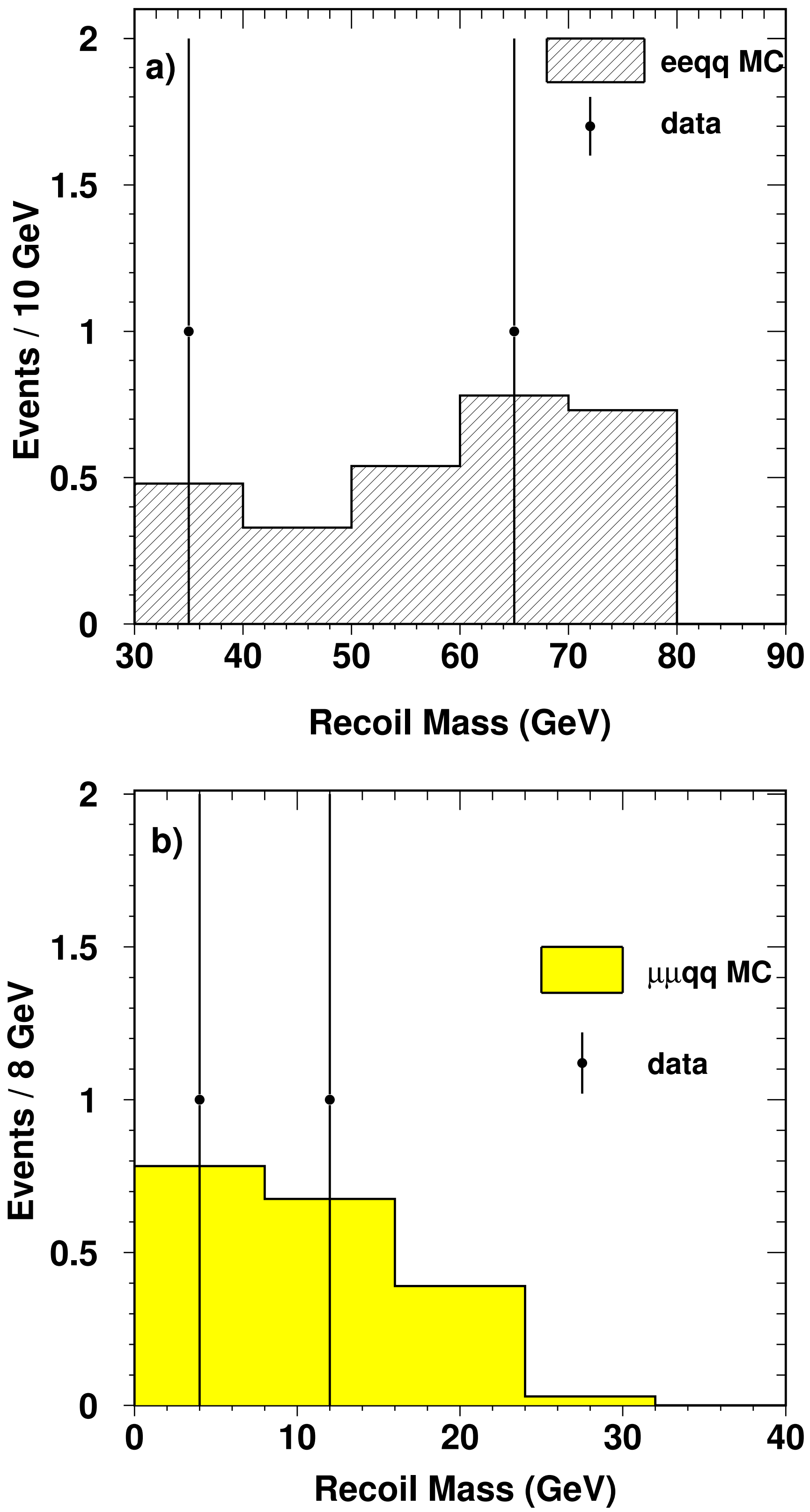

Figure 3: a) Distribution of the mass recoiling against the lepton pair for the expected four fermion background and data after the final high mass selection of the $H^0e^+e^-$ channel. b) The $\mu^+\mu^-$ recoil mass spectrum of the expected four fermion background and data for the low mass $H^0\mu^+\mu^-$ search.

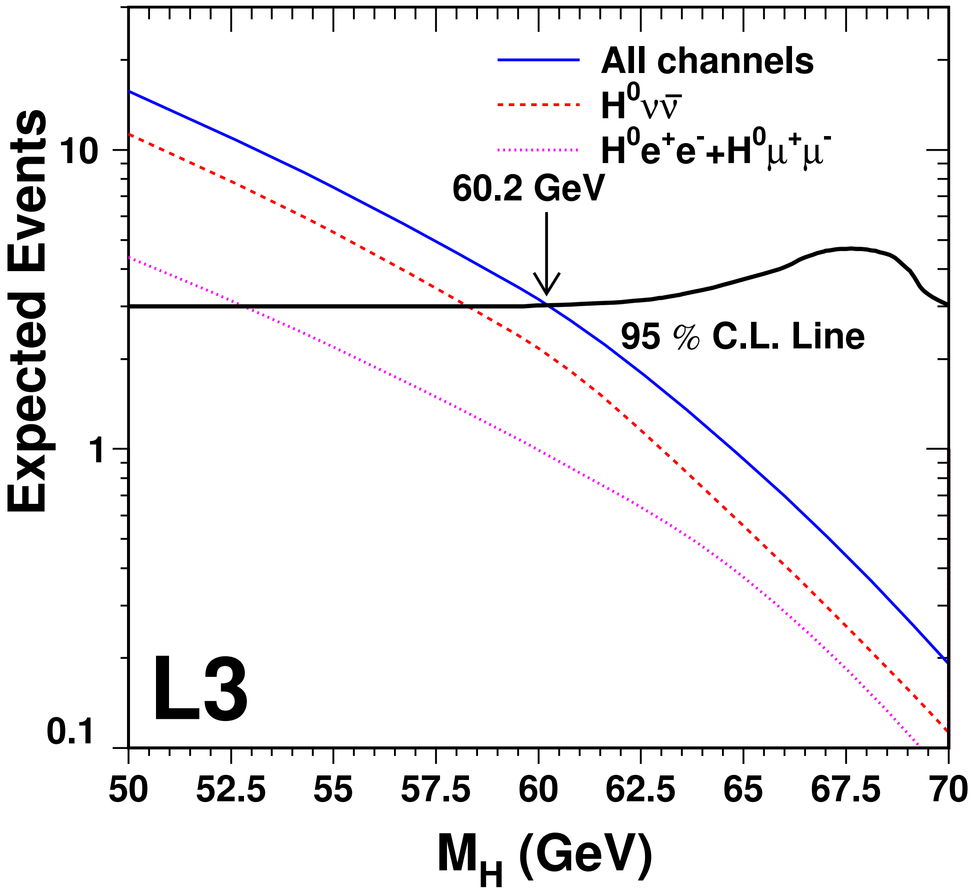

Figure 4: Number of Higgs events expected in the different channels and in all the channels together. The 95% confidence level line is shown with the Higgs mass limit at 60.2 GeV.

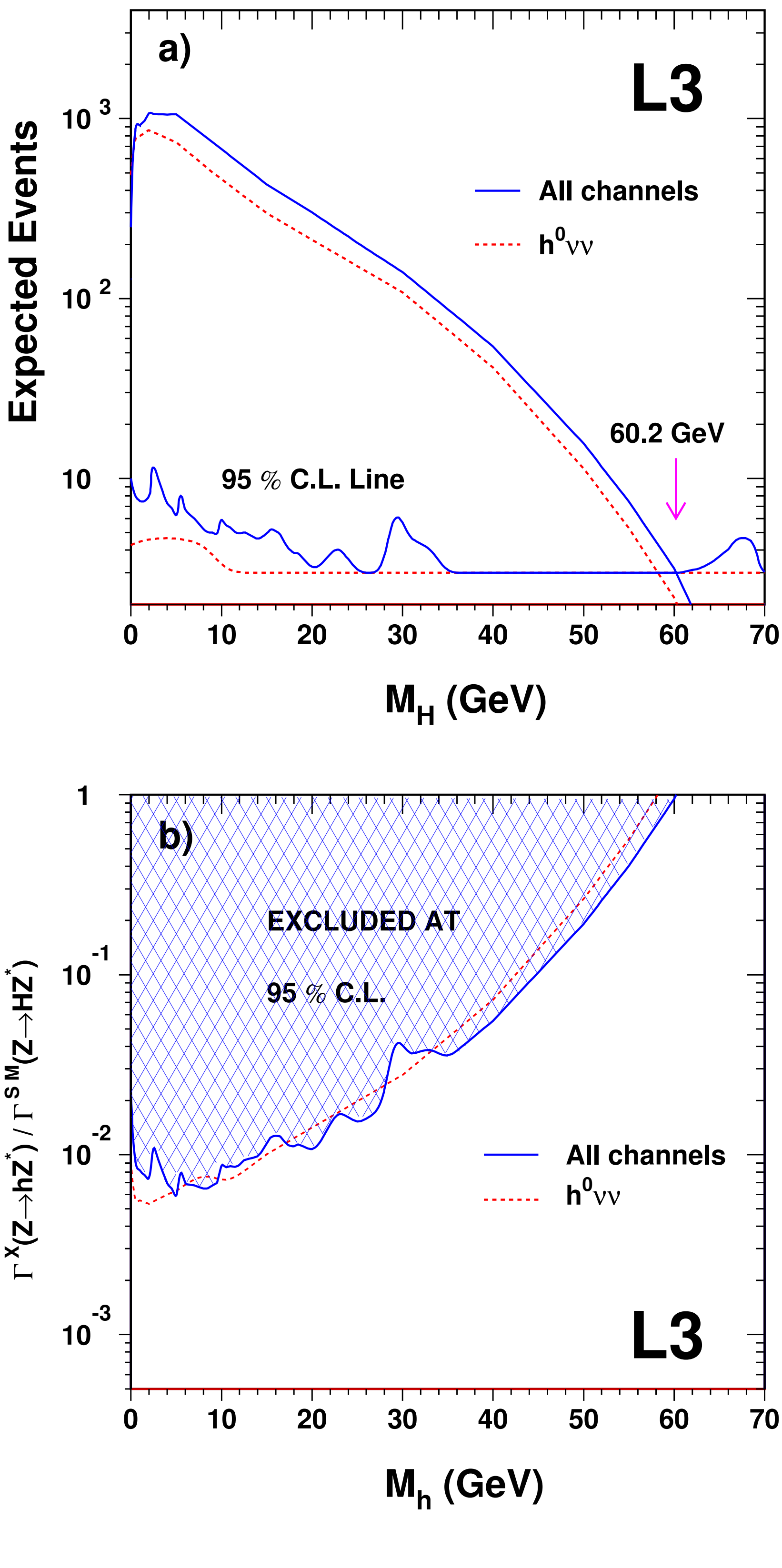

Figure 5: a) Number of Higgs events expected in the different channels as a function of the Higgs mass. The 95% confidence level line is shown with the Higgs mass limit at 60.2 GeV. b) 95% C.L. upper limit on the ratio between the cross section of the bremsstrahlung production of the Higgs boson in the Two Doublet Model and that of the SM Higgs boson. In the MSSM this ratio is equal to $\sin^2(\beta-\alpha)$.

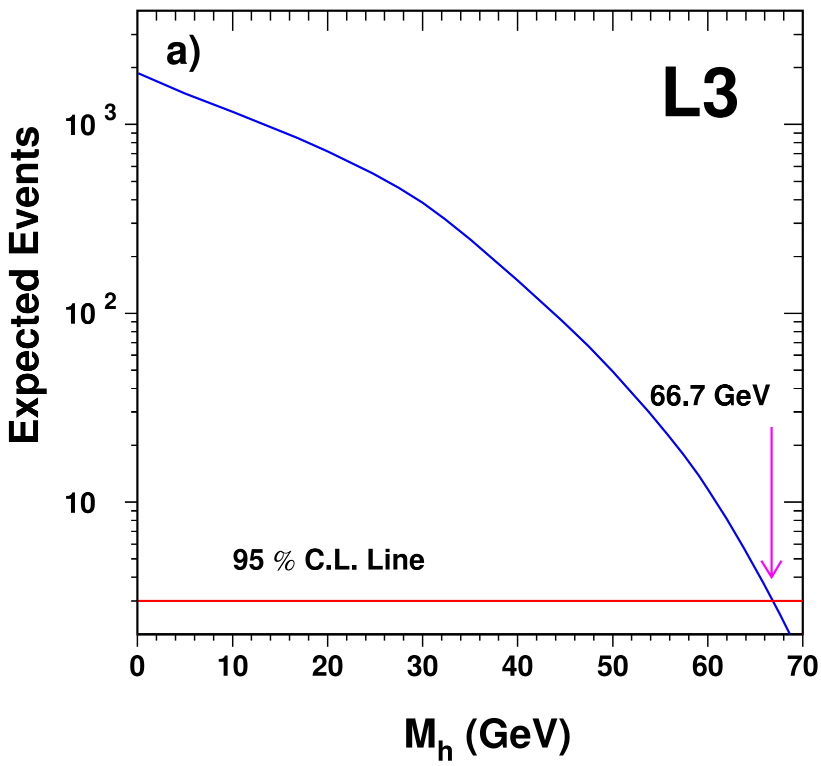

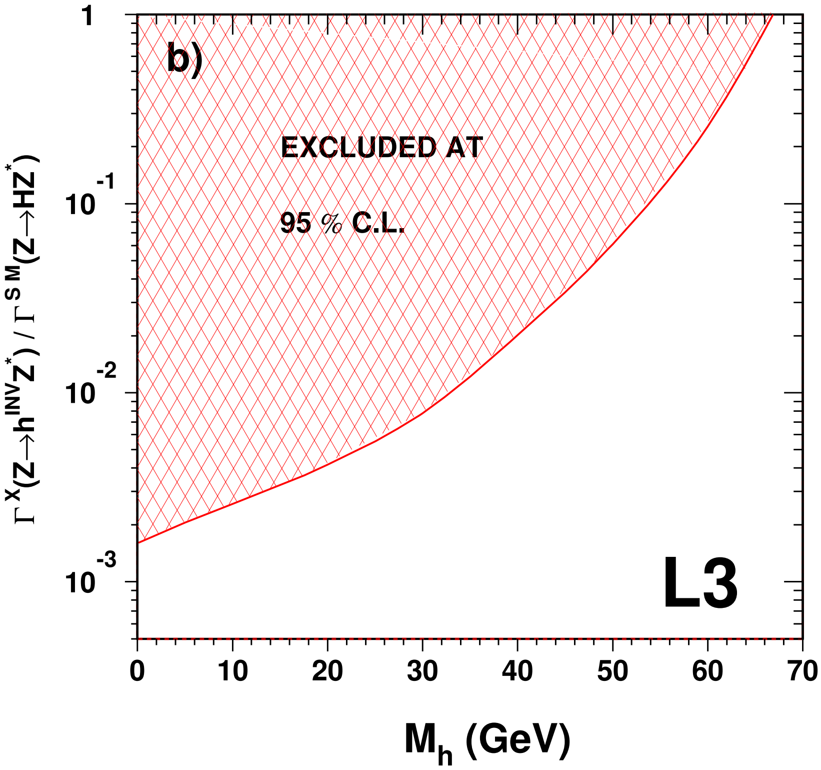

Figure 6: a) Number of events expected for Higgs invisible decays. The 95% confidence level line is shown with the Higgs mass limit at 66.7 GeV b) 95% C.L. upper limit on the ratio between the cross section of the bremsstrahlung production of an invisibly decaying Higgs boson and that of the SM Higgs boson.